Inorganic Chemistry

Article

Fabrication of Crystalline Mesoporous Metal Oxides and Sulfides

Keyan Xue, Dairong Chen,* and Xiuling Jiao

Key Laboratory for Special Functional Aggregate Materials of Education Ministry, School of Chemistry & Chemical Engineering, Shandong University, Jinan 250100 P. R. China

Mesoporous metal oxides and sulfides were prepared by a simple solvothermal method using inorganic salts as metal sources and diethylene glycol (DEG) as solvent; they are formed by the aggregation of metal compound nanoparticles. The generality of this route to the mesoporous materials was proved by the fabrication of a series of mesoporous materials (TiO$_2$, ZrO$_2$, ZnO, In$_2$O$_3$, ZnS, and In$_2$S$_3$). Due to the different morphologies of nanoparticle subunits, the as-prepared mesoporous materials had different types of mesopores, which could be revealed by the N$_2$ adsorption–desorption isotherms and transmission electron microscopy (TEM) images.

1. Introduction

In recent decades, mesoporous materials have attracted much attention for their potential applications in advanced catalysis, sensors, medicine, adsorbents, and nanodevices, etc.[1] Template methods including hard and soft templates routes have been frequently applied to prepare the mesoporous metal oxides and chalcogenides,[2] which have achieved great success in preparing mesostructured materials. However, for the large-scale and low-cost preparation of mesoporous materials, the template-free methods have become of interest, in which the sol–gel route is an effective one in fabricating mesoporous materials such as TiO$_2$, SnO$_2$, CeO$_2$, and MnO$_2$ by designing the reactive system.[3–7] The main impediment is the difficulty in controlling the competitive hydrolysis and condensation reactions, the decrease of the surface area of the products after calcination, and the expensive cost of metal alkoxides and complexes usually used as starting materials. In addition to the conventional sol–gel method, a nonhydrolytic sol–gel route has also been developed to prepare porous metal oxides materials.[8] To decrease the reaction temperature for the formation of mesoporous structure, hydrothermal treatment could be applied to replace the calcination in the sol–gel process.[9] As another typical template-free method, a one-step hydrothermal route to mesoporous TiO$_2$ derived from the metal salts and alkoxides was also introduced.[10] After that, Fujihara and co-workers fabricated crystalline mesoporous SnO$_2$ by a combined process including hydrolysis of SnCl$_4$ at 95 °C in alkaline solution, formation of SnO$_2$ nanocrystals, and subsequent hydrothermal treatment at 100–200 °C.[11] Most recently, many mesoporous aggregates such as Co$_3$O$_4$,[12] TiO$_2$,[13]

*To whom correspondence should be addressed. E-mail: cdr@sdu.edu.cn. Tel: 86-0531-88364280. Fax: 86-0531-88364281.

(1) (a) Schüth, F.; Schmidt, W. *Adv. Mater.* **2002**, *14*, 629. (b) Trewyn, B. G.; Gigi, S.; Slowing, I. I.; Lin, V. S. Y. *Chem. Commun.* **2007**, 3236. (c) Kanatzidis, M. G. *Adv. Mater.* **2007**, *19*, 1165. (d) Liang, C.; Li, Z.; Dai, S. *Angew. Chem., Int. Ed.* **2008**, *47*, 3696.
(2) (a) Lu, A.; Schüth, F. *Adv. Mater.* **2006**, *18*, 1793. (b) Lu, Y. *Angew. Chem., Int. Ed.* **2006**, *45*, 7664. (c) Yu, C.; Tian, B.; Zhao, D. *Curr. Opin. Solid State Mater. Sci.* **2003**, *7*, 191. (d) Dong, A.; Ren, N.; Tang, Y.; Wang, Y.; Zhang, Y.; Hua, W.; Gao, Z. *J. Am. Chem. Soc.* **2003**, *125*, 4976.
(3) (a) Pierre, A. C.; Pajonk, G. M. *Chem. Rev.* **2002**, *102*, 4243. (b) Arachchige, I. U.; Brock, S. L. *Acc. Chem. Res.* **2007**, *40*, 801.
(4) (a) Zhang, Y.; Weidenkaff, A.; Reller, A. *Mater. Lett.* **2002**, *54*, 375. (b) Phonthammachai, N.; Chairassameewong, T.; Gulari, E.; Jamieson, A. M.; Wongkasemjit, S. *Microporous Mesoporous Mater.* **2003**, *66*, 261. (c) Liu, C.; Fu, L.; Economy, J. *J. Mater. Chem.* **2004**, *14*, 1187. (d) Yang, L.; Zhu, L.; Liu, C.; Fang, M.; Liu, G.; Yu, X. *Mater. Res. Bull.* **2008**, *43*, 806. (e) Konishi, J.; Fujita, K.; Nakanishi, K.; Hirao, K. *Chem. Mater.* **2006**, *18*, 6069.
(5) (a) Velásquez, C.; Ojeda, M. L.; Campero, A.; Esparza, J. M.; Rojas, F. *Nanotechnology* **2006**, *17*, 3347. (b) Toupance, T.; Babot, O.; Jousseaume, B.; Vilacüa, G. *Chem. Mater.* **2003**, *15*, 4691. (c) Toupance, T.; Hamzaoui, H. E.; Jousseaume, B.; Riague, H.; Saadeddin, I.; Campet, G.; Brötz, J. *Chem. Mater.* **2006**, *18*, 6364.
(6) Phonthammachai, N.; Rumruangwong, M.; Gulari, E.; Jamieson, A. M.; Jitkarnka, S.; Wongkasemjit, S. *Colloids Surf. A* **2004**, *247*, 61.
(7) Hong, X.; Zhang, G.; Zhua, Y.; Yang, H. *Mater. Res. Bull.* **2003**, *38*, 1695.

(8) (a) Niederberger, M. *Acc. Chem. Res.* **2007**, *40*, 793. (b) Mutin, P. H.; Vioux, A. *Chem. Mater.* **2009**, *21*, 582. (c) Vioux, A. *Chem. Mater.* **1997**, *9*, 2292.
(9) (a) Raveendran, P.; Eswaramoorthy, M.; Bindu, U.; Chatterjee, M.; Hakuta, Y.; Kawanami, H.; Mizukami, F. *J. Phys. Chem. C* **2008**, *112*, 20007. (b) Wang, C.; Li, Q.; Wang, R. *Mater. Lett.* **2004**, *58*, 1424.
(10) (a) Ye, M.; Chen, Z.; Wang, W.; Zhen, L.; Shen, J. *Chem. Lett.* **2008**, *37*, 938. (b) Pavasupree, S.; Jitputti, J.; Ngamsinlapasathian, S.; Yoshikawa, S. *Mater. Res. Bull.* **2008**, *43*, 149.
(11) Fujihara, S.; Maeda, T.; Ohgi, H.; Hosono, E.; Imai, H.; Kim, S. *Langmuir* **2004**, *20*, 6476.
(12) He, T.; Chen, D.; Jiao, X. *Chem. Mater.* **2004**, *16*, 737.
(13) (a) Yu, J.; Zhang, L.; Yu, J. *New J. Chem.* **2002**, *26*, 416. (b) Yu, J.; Zhang, L.; Yu, J. *Chem. Mater.* **2002**, *14*, 4647. (c) Zhang, L.; Yu, J. *Chem. Commun.* **2003**, 2078. (d) Zhou, Y.; Antonietti, M. *J. Am. Chem. Soc.* **2003**, *125*, 14960. (e) Yu, J.; Zhang, L.; Cheng, B.; Su, Y. *J. Phys. Chem. C* **2007**, *111*, 10582. (f) Rossmanith, R.; Weiss, C. K.; Geserick, J.; Hüsing, N.; Hörmann, U.; Kaiser, U.; Landfester, K. *Chem. Mater.* **2008**, *20*, 5768. (g) Masuda, Y.; Kato, K. *Cryst. Growth Des.* **2008**, *8*, 3213. (h) Zhang, Y.; Li, G.; Wu, Y.; Luo, Y.; Zhang, L. *J. Phys. Chem. B* **2005**, *109*, 5478. (i) Lakshminarasimhan, N.; Bae, E.; Choi, W. *J. Phys. Chem. C* **2007**, *111*, 15244. (j) Deshpande, S. B.; Potdar, H. S.; Khollam, Y. B.; Patil, K. R.; Pasricha, R.; Jacob, N. E. *Mater. Chem. Phys.* **2006**, *97*, 207. (k) Yu, J.; Zhang, L.; Cheng, B.; Su, Y. *J. Phys. Chem. C* **2007**, *111*, 10582.

Table 1. Typical Preparation Parameters for the Different Mesoporous Materials

sample	reagents	volume of autoclave	reaction temperature and time	remarks[a]
SnO_2	0.703 g $SnCl_4 \cdot 5H_2O$, 24.0 mL DEG, 0.405 g NaOH	30.0 mL	200 °C, 12 h	
ZrO_2	0.322 g $ZrOCl_2 \cdot 8H_2O$, 12.0 mL DEG, 0.295 g NaOH	15.0 mL	200 °C, 12 h	
TiO_2	0.240 g $Ti(SO_4)_2$, 13.0 mL DEG, 2.0 mL water	15.0 mL	180 °C, 12 h	$Ti(SO_4)_2$ was dissolved in a mixture of DEG and water under magnetic stirring for 5 h
In_2O_3	0.767 g $In(NO_3)_3 \cdot 4H_2O$, 24.0 mL DEG	30.0 mL	200 °C, 12 h	
ZnO	0.301 g $Zn(NO_3)_2 \cdot 6H_2O$, 12.0 mL DEG	15.0 mL	200 °C, 12 h	
In_2S_3	0.301 g $Zn(NO_3)_2 \cdot 6H_2O$, 12.0 mL DEG, 0.152 g thiourea	15.0 mL	200 °C, 12 h	$InCl_3 \cdot 4H_2O$ was dissolved into a mixture of DEG and water, and then thiourea was added to be completely dissolved under stirring
ZnS	0.300 g $Zn(NO_3)_2 \cdot 6H_2O$, 25.0 mL DEG, 1.0 mL ammonia solution (25−28 wt %), 0.080 g thiourea	30.0 mL	180 °C, 8 h	Ammonia solution was added into $Zn(NO_3)_2 \cdot 6H_2O$ of DEG solution and then thiourea was added to form a solution

[a] All the solvothermal reaction products were collected by centrifugation, washed with water and ethanol for several times, and dried at 90 °C for 5 h. The yields of the products were 85.5%, 73.1%, 90.2%, 29.5%, 47.1%, 53.8%, and 83.2%, respectively, for mesoporous SnO_2, ZrO_2, TiO_2, In_2O_3, ZnO, In_2S_3, and ZnS.

N-doped TiO_2,[14] SnO_2,[15] α-Fe_2O_3,[16] γ-AlOOH,[17] Mg-$(OH)_2$,[18] and chalcogenides (ZnS, CdS, Ag_2S, Ag_2Se)[19] have been successfully prepared by a variety of template-free methods. However, these fabrications are accidental and difficult to extend to the syntheses of other mesoporous materials. In addition, for the preparation of mesoporous metal oxides and sulfides, there are some additional challenges because they are susceptible to hydrolysis, redox reactions, or phase transformations accompanied by thermal breakdown of mesostructures.[20]

The polyol method was initially described for the preparation of metals and alloys, in which the high-boiling alcohol (e.g., glycerol, glycol) was used to reduce the metal precursor. This method can be extended to prepare the oxide materials such as ZnO, Fe_2O_3, $CoAl_2O_4$, and Bi_2O_3,[21] which can be understood as a sol−gel process carried out at elevated temperature.

The polyols with high molecular weight are one type of important surfactants and are frequently applied as the templates in the sol−gel or aqueous solution processes for the fabrication of nanoporous materials,[22,23] but those with small molecular weight such as DEG can be applied as modifier to prepare the dispersed nanocrystals.[24] However, only a few mesoporous materials have been prepared using the polyols.[25] Herein, we present a general and simple procedure to fabricate the mesoporous crystalline metal oxides and sulfides using the inorganic salts as the metal sources and DEG as solvent, which is a sol−gel combined solvothermal process and suitable for the preparation of a series of mesoporous metal oxides and sulfides.

2. Experimental Section

2.1. Preparation. All the chemicals were of analytical grade and were used without further purification. DEG (water content 0.917%) was used as solvent, and the typical preparations for the different mesoporous materials are listed in Table 1.

2.2. Characterization. X-ray diffraction (XRD) patterns of the products were recorded on a Rigaku D/Max 2200PC diffractometer with a graphite monochromator and Cu Kα radiation (λ = 0.15418 nm). Morphologies and structures of the products were characterized via a field-emission scanning electron microscope (FE-SEM, JEOL JSM 6700F) and high-resolution TEM (HR-TEM, GEOL-2010) with an accelerating voltage of 200 kV. TG analyses were carried out to monitor the weight losses of the products at a heating rate of 10 °C/min from 25 to 800 or 1100 °C under air atmosphere (Mettler Toledo, TGA/SDTA 851e). To evaluate the thermal stability of mesoporous materials, the as-obtained oxides were heat-treated at 350 to 600 °C for 3−5 h in air atmosphere based on the thermo gravimetric (TG) curves with the heating rate of 5 °C/min, which are listed in Table 2. TG/mass spectrometric measurement (MS) (Netzsch STA449C/Balzers thermostar, atmosphere was 25.0 mL/min air, heating rate was 5 °C/min) was also applied to track the thermal degradation of mesoporous SnO_2. Fourier transform infrared (FT-IR) spectra were recorded on a Nicolet 5DX FT-IR spectrometer using KBr pellet technique in the range of 400−4000 cm^{-1}. N_2 adsorption−desorption isotherms of the products were measured on a QuandraSorb SI apparatus at the temperature of liquid nitrogen (−196 °C), the products were degassed at 90 °C for 10.0 h before measurements.

(14) Chi, B.; Zhao, L.; Jin, T. *J. Phys. Chem. C* **2007**, *111*, 6189.
(15) (a) Ho, S.; Wong, A.; Ho, G. *Cryst. Growth Des.* **2009**, *9*, 732. (b) Yang, S.; Gao, L. *J. Am. Ceram. Soc.* **2006**, *89*, 1742.
(16) (a) Wu, Z.; Yu, K.; Zhang, S.; Xie, Y. *J. Phys. Chem. C* **2008**, *112*, 11307. (b) Gou, X.; Wang, G.; Park, J.; Liu, H.; Yang, J. *Nanotechnology* **2008**, *19*, 125606.
(17) Mathieu, Y.; Lebeau, B.; Valtchev, V. *Langmuir* **2007**, *23*, 9435.
(18) Yu, J.; Xu, A.; Zhang, L.; Song, R.; Wu, L. *J. Phys. Chem. B* **2004**, *108*, 64.
(19) (a) Yang, J.; Peng, J. J.; Zou, R.; Peng, F.; Wang, H.; Yu, H.; Lee, J. *Nanotechnology* **2008**, *19*, 255603. (b) Hu, J.; Ren, L.; Guo, Y.; Liang, H.; Cao, A.; Wan, L.; Bai, C. *Angew. Chem., Int. Ed.* **2005**, *44*, 1269. (c) Wang, D.; Xie, T.; Peng, Q.; Li, Y. *J. Am. Chem. Soc.* **2008**, *130*, 4016. (d) Bao, N.; Shen, L.; Takata, T.; Domen, K. *Chem. Mater.* **2008**, *20*, 110.
(20) Li, J.; Zhao, X.; Yan, C. *Mater. Lett.* **2006**, *60*, 2896.
(21) (a) Jezequel, D.; Guenot, J.; Jouini, N.; Fievet, F. *J. Mater. Res.* **1994**, *10*, 77. (b) Merikhi, J.; Jungk, H. O.; Feldmann, C. *J. Mater. Chem.* **2000**, *10*, 1311. (c) Jungk, H. O.; Feldmann, C. *J. Mater. Res.* **2000**, *15*, 2244. (d) Merikhi, J.; Feldmann, C. *J. Mater. Sci.* **2001**, *36*, 297.
(22) Wang, S.; Gu, F.; Li, C.; Lü, M. *Cryst. Growth Des.* **2007**, *7*, 2670.
(23) (a) An, T.; Liu, J.; Li, G.; Zhang, S.; Zhao, H.; Zeng, X.; Sheng, G.; Fu, J. *Appl. Catal., A* **2008**, *350*, 237. (b) Oh, S.; Lu, L.; Lee, H. *Mater. Lett.* **2006**, *60*, 2795. (c) Yang, R.; Yu, H.; Li, M. *J. Mater. Sci. Lett.* **2003**, *22*, 1131. (d) Yusuf, M. M.; Chimoto, Y.; Imai, H.; Hirashima, H. *J. Sol-Gel Sci. Technol.* **2003**, *26*, 635. (e) Zhang, L.; Zhu, Y.; He, Y.; Li, W.; Sun, H. *Appl. Catal., B* **2003**, *40*, 287. (f) Tan, R.; He, Y.; Zhu, Y.; Xu, B.; Cao, L. *J. Mater. Sci.* **2003**, *38*, 3973.

(24) Feldmann, C.; Jungk, H.-O. *Angew. Chem., Int. Ed.* **2001**, *40*, 359.
(25) (a) Barick, K. C.; Aslam, M.; Dravid, V. P.; Bahadur, D. *J. Phys. Chem. C* **2008**, *112*, 15163. (b) Zhang, Q.; Chou, T.; Russo, B.; Jenekhe, S. A.; Cao, G. *Angew. Chem., Int. Ed.* **2008**, *47*, 2402.
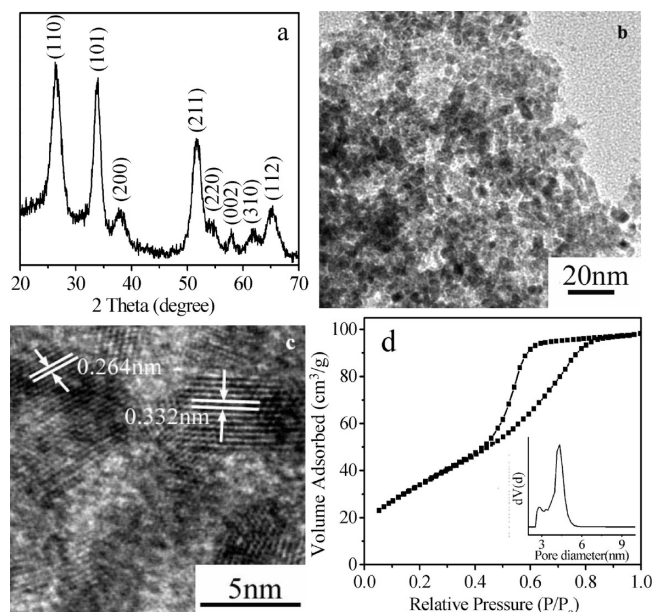
Figure 1. XRD pattern (a), HR-TEM images (b, c), and N_2 adsorption−desorption isotherms (d) of SnO_2 sample; the inset in d is the corresponding pore size distribution curve.

The density functional theory (DFT) method was used to calculate the pore size distribution due to its wide application of pore size ranging from micropore to mesopore. Gas chromatography−mass spectrometry (GC-MS, Agilent 6890N-5973N) was used to detect the byproduct in the system after solvothermal reaction.

3. Results and Discussion

As an example, the formation of SnO_2 sample was chosen to demonstrate the effectiveness of this route in preparing the mesoporous structures. The XRD pattern (Figure 1a) shows that all the reflections can be indexed to the tetragonal cassiterite phase of SnO_2 (JCPDS 41-1445, P42/mnm (136)) with lattice constant a = 4.738 Å, b = 4.738 Å, and c = 3.187 Å. Based on the breadth of (110) reflection, the average particle size calculated using the Scherrer formula is 5.1 nm. HR-TEM image (Figure 1b) indicates that the porous SnO_2 with mesopores of 5−8 nm is constructed by the nanocrystals of 5−10 nm which is roughly consistent with the size calculated from the corresponding XRD pattern. The lattice fringes of 0.332 and 0.264 nm can be ascribed to (110) and (101) planes respectively, revealing the cassiterite crystalline nature (Figure 1c). The lattice fringes also reveal that the SnO_2 nanocrystals aggregate in a disordered mode. N_2 adsorption−desorption isotherms show a type IV adsorption curve, indicating the mesoporous nature of SnO_2 sample (Figure 1d).[26] The calculated Brunauer−Emmett−Teller (BET) surface area and pore volume are 129 m^2/g and 0.142 cm^3/g. The hysteresis loop with a smoothly increasing adsorption branch and a somewhat steeper desorption branch is similar to the type H2 hyteresis loop, demonstrating that the product has cul-desac mesopores with some small variation along the pores.[27] The pore size distribution calculated by the DFT method is narrow and the mouth size of cul-desac pores is ca. 4.3 nm.
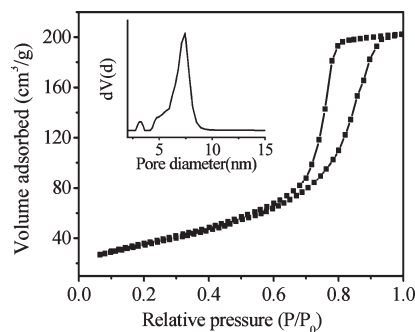

Figure 2. N_2 adsorption−desorption isotherm of the mesoporous SnO_2 calcined at 600 °C for 5 h, the inset is the corresponding DFT pore size distribution curve.
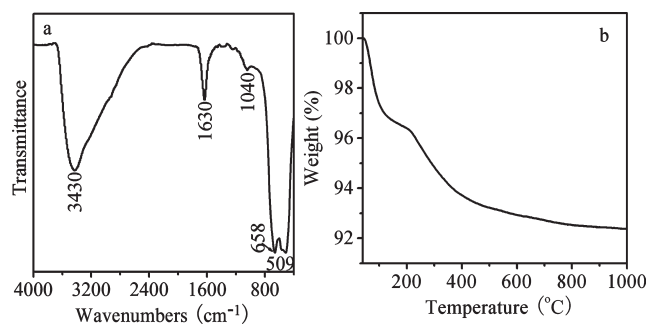

Figure 3. FT-IR spectrum (a) and TG curve (b) of mesoporous SnO_2.

Normally, the pores in the materials easily collapse at high temperature, which limits their applications. Here, the N_2 adsorption−desorption isotherms of the sample calcined at 600 °C for 5 h (Figure 2) exhibit a type-IV adsorption branch with an H2 type hysteresis loop similar to that of the uncalcined sample, indicating that the mesopores with morphology similar to that of uncalcined sample still remain after calcination.[26,27] The BET surface area is 125 m^2/g; this is close to that of the uncalcined sample, but the pore volume significantly increases to 0.302 cm^3/g. The pore size of ca. 7.4 nm calculated by the DFT method shows a slight enlarging of mesopores. The increase of the pore size and volume comparing to those of uncalcined one is due to the removal of hydroxyls and DEG species in the pores at high temperature which can be estimated from the TG curve (Figure 3b). Thus the mesoporous SnO_2 after calcination would maintain the BET surface area hardly changing with larger pore size and volume, demonstrating its high thermal stability.

As known, the DEG molecules can coordinate with many metal cations under the evaluated temperature,[28] it is speculated that the formation of mesoporous SnO_2 is related to the coordination of DEG to Sn^{4+} cations in the present system. GC-MS characterization indicates that the byproduct is 12-crown-4 (dehydrated compound of DEG, 22.90%) in the solution after solvothermal reaction (Supporting Information, Figure S1). In the present system, the crown ether might be formed by the condensation of DEG under the directing of Na^+ and Sn^{4+}, with water simultaneously produced. After then, the Sn^{4+} cations hydrolyzed to form SnO_2

(26) Kruk, M.; Jaroniec, M. *Chem. Mater.* **2001**, *13*, 3169.
(27) Wallacher, D.; Künzner, N.; Kovalev, D.; Knorr, N.; Knorr, K. *Phys. Rev. Lett.* **2004**, *92*, 195704−1.

(28) (a) Yang, J.; Li, C.; Quan, Z.; Kong, D.; Zhang, X.; Yang, P.; Lin, J. *Cryst. Growth Des.* **2008**, *8*, 695. (b) Hu, Y.; Ge, J.; Sun, Y.; Zhang, T.; Yin, Y. *Nano Lett.* **2007**, *7*, 1832. (c) Feldmann, C. *Adv. Funct. Mater.* **2003**, *13*, 101. (d) Prevot, V.; Forano, C.; Besse, J. P. *Chem. Mater.* **2005**, *17*, 6695. (e) Zhao, J.; Fan, W.; Wu, D.; Sun, Y. *J. Non-Cryst. Solids* **2000**, *261*, 15.

nanoparticles, some absorbed water, hydroxyls, and DEG molecules would exist on the surfaces of nanocrystals due to the coordination of DEG molecules to Sn^{4+} cations, which could be confirmed by the IR spectra, TG curve, and elemental analyses. To decrease the high surface energy, the nanocrystals would aggregate to the mesoporous SnO_2 because the DEG molecules on the surface prevented the nanoparticles from densely aggregating.

FT-IR spectrum of the as-prepared mesoporous SnO_2 (Figure 3a) shows a strong and wide band at 3430 cm^{-1} with a shoulder at ca. 2900 cm^{-1} and absorptions at 1630, 1040, 658, and 509 cm^{-1}. The strong absorptions at 3430 and 1630 cm^{-1} can be attributed to the stretching and bending modes of hydroxyls in water and DEG, as well as the hydroxyls bonded to Sn^{4+} cations.[29a] According to those of DEG molecules (Figure 6a), the IR absorptions at ca. 2900 and 1040 cm^{-1} are respectively ascribed to the vibrations of C−H and C−O in DEG molecules, and those at 658 and 509 cm^{-1} are assigned to the Sn−O vibrations.[29b] Compared to that in pure DEG, the IR absorption of C−O bond in the as-prepared SnO_2 shifts ca. 20 cm^{-1} to lower wavenumbers, indicating that there is chemical interaction between the DEG molecules and Sn^{4+} cations.[30b] The absence of the absorptions at ca. 1250 and 950−810 cm^{-1} reveals that the organics in the mesoporous SnO_2 is DEG rather than 12-crown-4, but the weak absorptions at 1040 cm^{-1} indicates that there are only a few DEG molecules in the product. TG analysis (Figure 3b) shows a weight loss of 3.0% below 150 °C and another one of ca. 4.5% at temperature higher than 150 °C. TG/MS analysis shows that the water has been lost in the measured temperature range and the curve has a small hump at 150−400 °C (Supporting Information, Figure S2, denoted with the arrow), but the CO_2 has been released ranging from 150 °C to ca. 400 °C. It is known that the boiling point and flash point of DEG are, respectively, 244.8 and 135 °C, and those of 12-crown-4 are relatively higher. Thus it can be concluded that the weight loss at the temperature lower than 150 °C is mainly due to the removal of the physically and chemically absorbed water; the decomposition of DEG molecules occurs from 150 to 400 °C to release water and CO_2, which overlaps with the removal of water in the mesopores,[31] and the small weight loss at the temperature higher than 400 °C is related to the release of water from surface hydroxyls.[32] The elemental analysis gave that the C, H, and N contents are 0.470%, 1.125%, and 0.268%, in which the N is derived from the absorbed N_2. It is concluded that there is ca. 1.04% DEG in the product, and the other weight loss of ca. 6.6% is attributed to the removal of the absorbed hydroxyls by treatment at high temperature.

It is presumed that this may be a general route to mesoporous materials by the aggregation of nanoparticles because many metal cations can coordinate to DEG molecules.[28] To confirm its generality, the fabrication of several
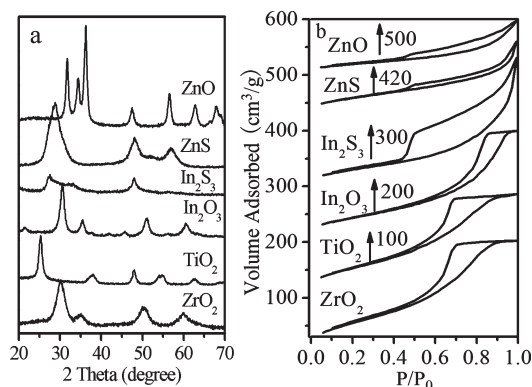

Figure 4. XRD patterns (a) and N_2 adsorption−desorption isotherms (b) of mesoporous ZnO, TiO_2, ZrO_2, In_2O_3, ZnS, and In_2S_3.

mesoporous materials (TiO_2, ZrO_2, ZnO, In_2O_3, ZnS, and In_2S_3) by this route was investigated. The XRD patterns (Figure 4a) indicate that all the as-prepared samples are phase-pure materials, Table 2 gives their corresponding crystalline structures. The products have high crystallinity except In_2S_3, which is similar to the previously reported In_2S_3 nanostructures and might be related to its internal structure.[33] Compared with the respective standard XRD patterns, the wider reflections reveal that the as-prepared materials are composed of small crystalline particles. Based on the breadth of reflections, the particle sizes of the as-prepared TiO_2, ZrO_2, ZnO, In_2O_3, and ZnS are calculated to be 9.0, 3.4, 10.0, 6.2, and 3.8 nm, respectively. In addition, the ZrO_2 sample exhibiting the cubic structure rather than the familiar monoclinic phase may be due to the size effect. All the N_2 adsorption−desorption isotherms (Figure 4b) show type IV adsorption branches, indicating the mesoporous natures of the products.[26] This means that all the samples are mesoporous materials, demonstrating the generality of this synthetic method.

The types of hysteresis loops also imply that the samples have different kinds of mesopores (Figure 4b). Like SnO_2, the mesoporous ZrO_2, TiO_2, and In_2O_3 exhibit hysteresis loops similar to type H2, indicating the existence of cul-desac mesopores.[27] The narrow DFT pore size distribution curves give the mouth pores of 5.4 nm in ZrO_2 and TiO_2 samples, however, the In_2O_3 sample with a main mouth pore of 8.5 nm has the wider pore size distribution, and its typical hysteresis loop of type H3 indicates slit-like pores existing in the sample, which might be due to the loose aggregates of plate-like particles (Table 2, Supporting Information, Figure S3).[26,27] The pore size of ca. 4.0 nm should be assigned to the slit size between the plate-like particles. The outlines of the hysteresis loops of the ZnO and ZnS samples demonstrate that they have different kinds of coexisting mesopores. In previous reports, besides the crystalline mesoporous TiO_2 and SnO_2 prepared by template-free hydrothermal/solvothermal routes had higher surface area than 200 m^2/g,[9a] most of the mesoporous materials showed a relatively low surface area or wide pore size distribution, and no report focused on the general route to mesoporous materials ranging from oxides to sulfides.

HR-TEM and FE-SEM images show that the ZrO_2, TiO_2, ZnO, In_2O_3, and ZnS samples have morphologies and

(29) (a) Nakamoto, K. *Infrared and Raman Spectra of Inorganic and Coordination Compounds* (in Chinese; Huang, D.; , Wang, R., Translators); 4th Chemical Industry Press: Beijing, 1991, p 251. (b) Dharmaraj, N.; Kim, C.; Kim, K.; Kim, H.; Suh, E. *Spectrochim. Acta Part A* **2006**, *64*, 136.

(30) (a) Xu, Y.; Jiao, X.; Chen, D. *J. Phys. Chem. C* **2008**, *112*, 16769. (b) Xu, Y.; Jiao, X.; Chen, D. *J. Phys. Chem. C* **2007**, *111*, 16284. (c) Gou, L.; Murphy, C. J. *J. Mater. Chem.* **2004**, *14*, 735.
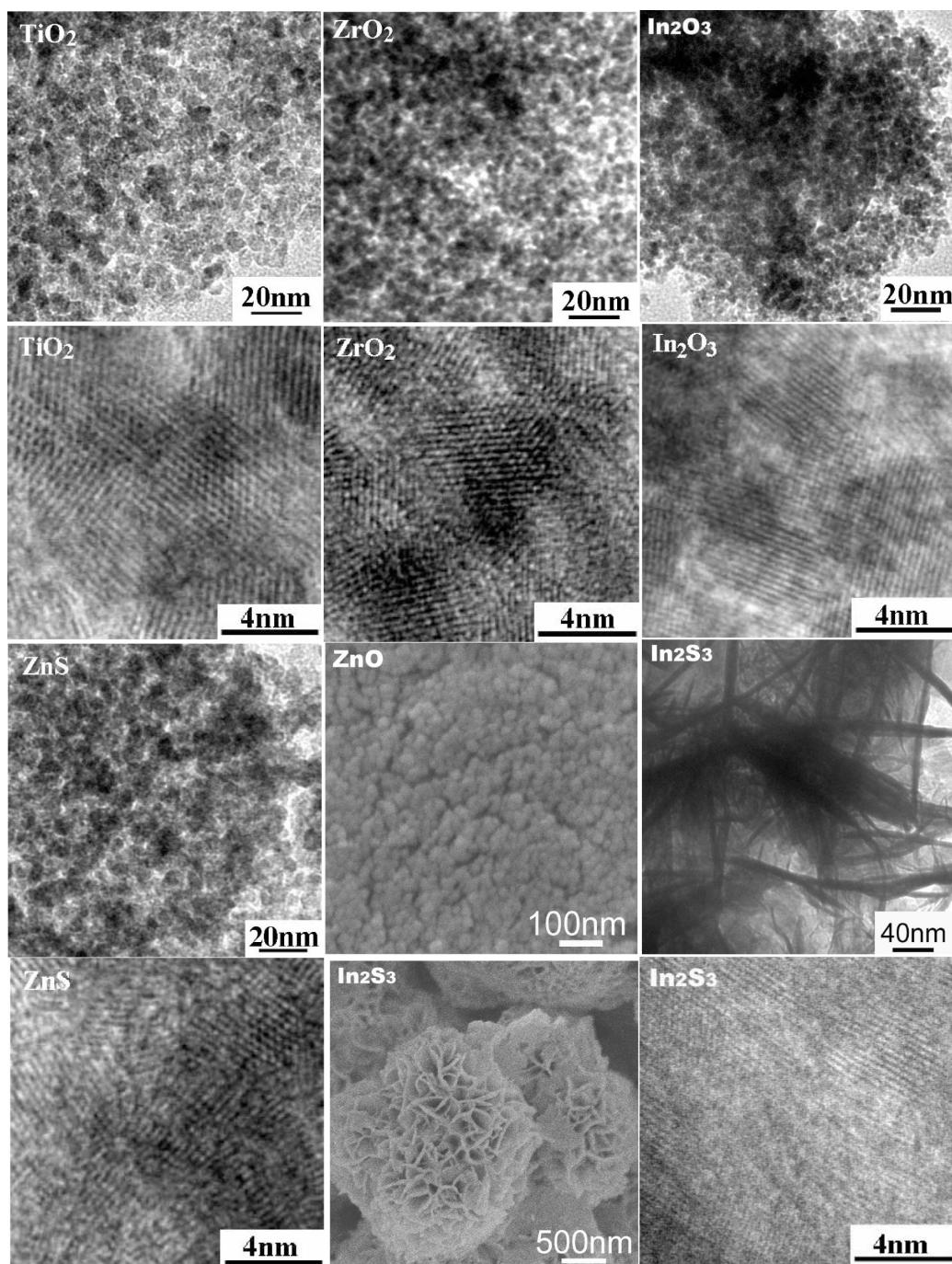
(31) Jitianu, A.; Altindag, Y.; Zaharescu, M.; Wark, M. *J. Sol-Gel Sci. Technol.* **2003**, *26*, 483.

(32) Monredon, S.; Cellot, A.; Ribot, F.; Sanchez, C.; Armelao, L.; Gueneau, L.; Delattre, L. *J. Mater. Chem.* **2002**, *12*, 2396.

(33) (a) Du, W.; Zhu, J.; Li, S.; Qian, X. *Cryst. Growth Des.* **2008**, *8*, 2130. (b) Chen, L.; Zhang, Z.; Wang, W. *J. Phys. Chem. C* **2008**, *112*, 4117.

Table 2. Properties of the As-Prepared Mesoporous Materials

sample	phase structure (by XRD)	specific surface area (m^2/g)		pore size (nm)		calcination	
		before calcination	after calcination	before calcination	after calcination	temperature (°C)	time(h)
ZrO_2	cubic	210	143	5.4	7.9	450	3
In_2O_3	cubic	160	135	8.5	8.5	400	5
TiO_2	anatase	198	99	5.4	7.1	450	3
ZnO	wurtzite	71	53	3.8	7.8	350	3
ZnS	cubic	138		3.8			
In_2S_3	cubic	117		4.0			

Figure 5. HR-TEM and FE-SEM images of the as-prepared mesoporous materials.

microstructures similar to those of mesoporous SnO_2 which is the aggregate of spherical nanocrystals of 4−8 nm. As to

the mesoporous In_2S_3 with flower-like architectures, the nanoplate subunits with thickness of ca. 5−7 nm construct
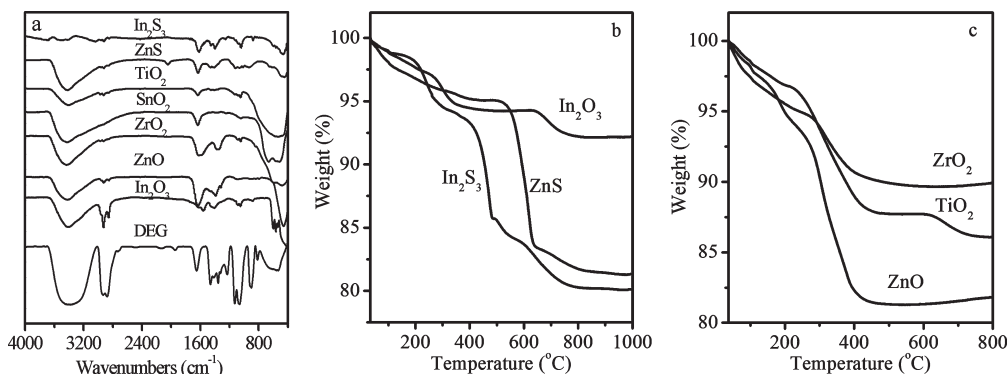
Figure 6. FT-IR spectra of mesoporous materials and DEG (a) and TG curves of mesoporous materials (b, c).
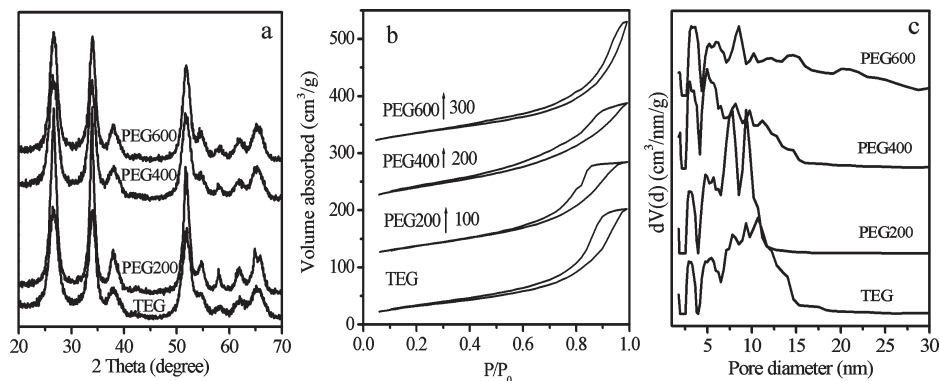

Figure 7. XRD patterns (a), N_2 adsorption−desorption isotherms (b), and pore size distribution (c) curves of mesoporous SnO_2 prepared from different PEG solvents.

the slit-like pores, this could also be confirmed by the N_2 adsorption−desorption analysis. Furthermore, the obvious relative departure of the lattice fringes although the continuous lattice fringes in a single nanoplate indicate the nanoplate forming through an oriented attachment of the nanocrystals (Figure 5).

All the samples show IR absorptions similar to the SnO_2 sample in the wavenumber range of 1000−4000 cm^{-1}, indicating that all the products have absorbed water, surface hydroxyls, and DEG; however, the difference in the relative IR absorptions intensity reveals their different contents (Figure 6a). The similar species on the nanoparticle subunits' surface also indicate that all the products are formed through a similar mechanism. Elemental analyses show that the DEG contents are respectively 2.79%, 3.16%, 2.99%, 12.13%, 1.64%, and 4.27% in mesoporous ZrO_2, In_2O_3, TiO_2, ZnO, ZnS, and In_2S_3 (Table S1). In addition, there are a few of the absorbed air, water, and hydroxyls in the products. The TG curves also indicate the different weight losses in the temperature ranging from room temperature to 800 or 1000 °C (Figure 6b, c). The In_2O_3, ZrO_2, TiO_2, and ZnO samples have weight losses of ca. 8%, 10.5%, 14%, and 19% indicating that the absorbed air, water, and hydroxyls except DEG are ca. 4.84%, 7.71%, 11.01%, and 6.87%, respectively. As for the mesoporous In_2S_3 and ZnS, the oxidation reaction to metal oxides that have the weight loss of 14.8% and 16.4% should occur in the thermogravimetric process. Thus it can be concluded that the absorbed air, water, and DEG in In_2S_3 and ZnS are ca. 5.2% and 2.1%, respectively, of which the absorbed air and water are ca. 1% and 0.5%. The different contents of water, hydroxyls, and DEG in the mesoporous

materials might be due to their different surface areas and coordination abilities to DEG molecules and hydroxyls.

Because a variety of polyols exhibit similar complexing ability to the metal cations,[30] it is speculated that the mesoporous materials can be formed by using other polyols as solvents. Thus TEG (triethylene glycol), PEG200, PEG400, and PEG600 were also selected as solvents to prepare the mesoporous SnO_2. The XRD patterns (Figure 7a) show that all the reflections can be indexed to the tetragonal cassiterite phase of SnO_2, which means that the crystalline SnO_2 can be formed in TEG, PEG200, PEG400, or PEG600 solution. The N_2 adsorption−desorption isotherms (Figure 7b) exhibit the type IV adsorption branch, proving the mesoporous nature (Figure 7c). The specific surface areas of the samples calculated by BET method vary from 120 to 154 m^2/g (Supporting Information, Table S2). However, all the samples show wide pore size distributions with most of the pores less than 15 nm. Moreover, the pore size distributions broaden with the increase of the molecule weight of PEG, which may be due to the broad molecular weight distribution and more flexibility of molecule chains. This shows that the solvothermal route using polyols as solvent and structure directing agent may be a general route to mesoporous materials.

4. Conclusions

In summary, a general route to the mesoporous metal oxides and sulfides has been developed using the metal inorganic salts as metal sources and DEG as solvent. The formation of mesoporous materials went through the formation of metal compound nanoparticles and their aggregation, in which DEG species on the nanoparticles'

surface prevent the nanoparticles from densely aggregating and then the mesostructures are formed. The mesoporous materials exhibit different pore sizes, morphologies, and pore size distributions because of the different sizes and shapes of composed nanoparticles. After calcinations to remove the organics, the pore structures of metal oxides could still be maintained although their surface areas decreased.

Supporting Information Available: GC-MAS, TGA-MAS of the mesoporous SnO_2, DFT pore size distribution curves, elemental analyses results of the as-prepared ZrO_2, In_2O_3, TiO_2, ZnO, ZnS and In_2S_3, the specific surface areas and pore volumes of the SnO_2 prepared in TEG, PEG200, PEG400, PEG600. This material is available free of charge via the Internet at http://pubs.acs.org.